

UC Irvine

UC Irvine Previously Published Works

Title

The changing influences of ENSO and the Pacific Meridional Mode on mesoscale eddies in the South China Sea
The changing influences of ENSO and the Pacific Meridional Mode on mesoscale eddies in the South China Sea

Permalink

<https://escholarship.org/uc/item/76k819xw>

Journal

Journal of Climate, 32(3)

ISSN

0894-8755

Authors

Tuo, Pengfei

Yu, Jin-Yi

Hu, Jianyu

Publication Date

2019-02-01

DOI

10.1175/jcli-d-18-0187.1

Copyright Information

This work is made available under the terms of a Creative Commons Attribution License, available at <https://creativecommons.org/licenses/by/4.0/>

Peer reviewed

The Changing Influences of ENSO and the Pacific Meridional Mode on Mesoscale Eddies in the South China Sea

PENGFEI TUO

State Key Laboratory of Marine Environmental Science, College of Ocean and Earth Sciences, Xiamen University, Xiamen, China, and Department of Earth System Science, University of California, Irvine, Irvine, California

JIN-YI YU

Department of Earth System Science, University of California, Irvine, Irvine, California

JIANYU HU

State Key Laboratory of Marine Environmental Science, College of Ocean and Earth Sciences, Xiamen University, Xiamen, China

(Manuscript received 28 March 2018, in final form 8 October 2018)


ABSTRACT

This study finds that the correlation between El Niño–Southern Oscillation (ENSO) and the activity of mesoscale oceanic eddies in the South China Sea (SCS) changed around 2004. The mesoscale eddy number determined from satellite altimetry observations using a geometry of the velocity vector method was significantly and negatively correlated with the Niño-3.4 index before 2004, but the correlation weakened and became insignificant afterward. Further analyses reveal that the ENSO–eddy relation is controlled by two major wind stress forcing mechanisms: one directly related to ENSO and the other indirectly related to ENSO through its subtropical precursor—the Pacific meridional modes (PMMs). Both mechanisms induce wind stress curl variations over the SCS that link ENSO to SCS eddy activities. While the direct ENSO mechanism always induces a negative ENSO–eddy correlation through the Walker circulation, the indirect mechanism is dominated by the northern PMM (nPMM), resulting in a negative ENSO–eddy correlation before 2004, and by the southern PMM (sPMM) after 2004, resulting in a positive ENSO–eddy correlation. As a result, the direct and indirect mechanisms enhance each other to produce a significant ENSO–eddy relation before 2004, but they cancel each other out, resulting in a weak ENSO–eddy relation afterward. The relative strengths of the northern and southern PMMs are the key to determining the ENSO–eddy relation and may be related to a phase change of the interdecadal Pacific oscillation.

1. Introduction

The South China Sea (SCS) is a semienclosed sea located in the subtropical western Pacific whose upper-ocean circulation is strongly influenced by surface winds in the region (e.g., Fang et al. 1998; Chu et al. 1999; Hu et al. 2000; Fang et al. 2002; Liu et al. 2008; Hu and Wang 2016). The winds produce stress and stress curls that directly drive ocean currents within the basin as well as

modulate Kuroshio intrusions into the basin through the Luzon Strait, both of which are the primary factors in determining the circulation pattern in the SCS (e.g., Farris and Wimbush 1996; Qu 2000; Qu et al. 2004; Yuan et al. 2006; Wang et al. 2013). The surface wind patterns vary seasonally in association with the seasonal reversal of the East Asian monsoon (e.g., Ding et al. 2004; Wang et al. 2009) and interannually in association with the occurrence of El Niño–Southern Oscillation (ENSO) events (e.g., Chao et al. 1996; B. Wang et al. 2000; Qu et al. 2004, 2005; C. Wang et al. 2006; Y. Wang et al. 2006). During ENSO events, anomalous warming and cooling of the sea surface in the central-to-eastern tropical Pacific can disturb the atmospheric circulation, resulting in sea surface wind variations over a large part

 Denotes content that is immediately available upon publication as open access.

Corresponding author: Jin-Yi Yu, jyyu@uci.edu; Jianyu Hu, hujy@xmu.edu.cn.

DOI: 10.1175/JCLI-D-18-0187.1

© 2019 American Meteorological Society. For information regarding reuse of this content and general copyright information, consult the [AMS Copyright Policy \(www.ametsoc.org/PUBSReuseLicenses\)](https://www.ametsoc.org/PUBSReuseLicenses).

of the Pacific Ocean, including the SCS region (e.g., Zhang et al. 1997; C. Wang et al. 2006; Fang et al. 2006; Wang et al. 2009). The Luzon throughflow can also convey the ENSO influence into the interior SCS (Farris and Wimbush 1996; Qu et al. 2004, 2009; Nan et al. 2015).

Surface wind variations over the SCS affect not only the large-scale circulation but also the mesoscale ocean eddies inside the basin. Mesoscale eddies can be observed throughout the SCS (e.g., Soong et al. 1995; Li et al. 1998; Shaw et al. 1999; Wang et al. 2003; Yuan et al. 2007; D. Wang et al. 2008; Xiu et al. 2010; Chen et al. 2011; Lin et al. 2015; Xia and Shen 2015) and have a typical radius of about 100–200 km and a typical lifespan of approximately 8–10 weeks (Chen et al. 2011). Despite their chaotic nature, mesoscale ocean eddies play an essential role in transporting water mass, energy, and biochemical substances into the interior SCS and can profoundly impact the regional climate and environment (e.g., Hwang and Chen 2000; Wang et al. 2003; Xiu et al. 2010; Chen et al. 2011). Previous studies have suggested that mesoscale eddies in the SCS can be generated via baroclinic instability of the gyre circulation within the basin (Pedlosky 1982; Wu et al. 1999; L. Wang et al. 2000; Cheng and Qi 2010; Sun et al. 2016) that is forced by the monsoonal flows, the interactions between the monsoonal flows and coastal topography (Wang et al. 2003; G. Wang et al. 2008; Chen et al. 2010; Chu et al. 2017), and by the frontal instability (Wang et al. 2003; Gan and Qu 2008) or vorticity advection associated with Kuroshio intrusions (Metzger and Hurlburt 2001; Jia and Chassignet 2011; Nof et al. 2011). Each of these eddy-generation mechanisms is directly or indirectly related to the prevailing wind stress and wind stress curls over the SCS. Variations in surface winds induced by remote forcings, such as those associated with ENSO, can strengthen or weaken the gyre instability or Kuroshio intrusions to modulate the SCS eddy activity. Mesoscale eddies respond to wind forcing rather rapidly with a response time of about one to several weeks (Chi et al. 1998; G. Wang et al. 2008; Chu et al. 2017).

ENSO is a key contributor to the interannual variability in surface winds over the SCS, which in turn should enable ENSO to influence the mesoscale eddy activity in the SCS. However, previous studies were not conclusive concerning the relationship between ENSO and SCS mesoscale eddy activity. Cheng and Qi (2010), for example, found the level of eddy kinetic energy (EKE) in the SCS to be below normal during El Niño events but above normal during La Niña events. They argued that El Niño (La Niña) events can induce anomalous anticyclonic (cyclonic) wind stress curl over the SCS, which weakens (strengthens) the background cyclonic gyre, giving rise to a below- (above) normal level

of eddy activity during El Niño (La Niña) events. ENSO can also affect the mesoscale eddy activity in the SCS by modulating the Kuroshio intrusions into the basin. Typically, El Niño events weaken the Kuroshio intrusions (Metzger and Hurlburt 2001; Metzger 2003; Qu et al. 2004), which reduces frontal instability and/or vorticity advection into the SCS (Cheng and Qi 2010; Nan et al. 2015) and consequently reduces eddy activity in the SCS; and vice versa for La Niña events (Jia and Chassignet 2011; Nof et al. 2011; Nan et al. 2015). ENSO is also suggested to affect the summer monsoon flow that modulates the wind stress curl pattern off Vietnam and thus affects the eddy activity in the SCS (Chu et al. 2017). However, there were studies that suggest that the ENSO impact on the SCS eddies is weak or not clear. Xiu et al. (2010) employed a numerical model to examine the relationship between ENSO and the eddy number and found no direct correlation. Chen et al. (2011) found no obvious correlation between ENSO and the SCS eddy number they identified from satellite observations. The different findings on the ENSO–eddy relationship may be caused by the different datasets or identification methods used in the studies, or they may be due to the existence of decadal changes in the ENSO–eddy relationship.

Because of their random and chaotic characteristics, mesoscale eddies are not easy to directly identify from observations. In this study, we employ an automatic eddy identification method based on the geometry of velocity (GV) field (Nencioli et al. 2010) to determine the mesoscale eddy number in the SCS from satellite altimetry observations. The GV method has been shown to determine the eddy number with reasonably good accuracy (Lin et al. 2015; Xia and Shen 2015) compared with other methods (Wang et al. 2003; Xiu et al. 2010; Chen et al. 2011). We then use the identified eddy number to examine the relationship between ENSO and SCS mesoscale eddy activity. We discovered that the ENSO–eddy relationship is not stationary but changes from decade to decade. Furthermore, we find the mesoscale eddy activity in the SCS is also affected by the remote forcing from an ENSO precursor—the Pacific meridional modes (PMMs) in the subtropical Pacific of both hemispheres. The subtropical Pacific influences, which were not emphasized by previous studies, are a reason why the ENSO–eddy relationship changes over the decades. The large-scale dynamical mechanisms that link SCS mesoscale eddies to ENSO and the PMMs are then identified and explained.

This paper is organized as follows: Data and the method for identifying mesoscale eddies used in this paper are introduced in section 2. The wind stress curl modes and associated large-scale atmospheric and

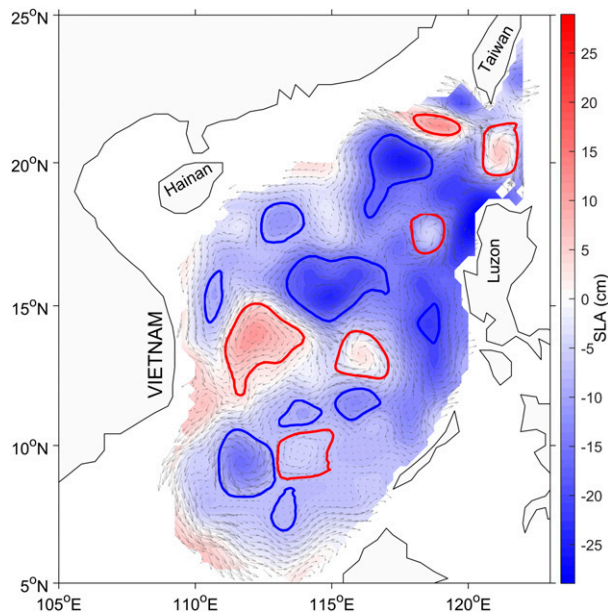


FIG. 1. The mesoscale eddies identified by the GV method using the SLA (contour; cm) and current (vectors; cm s^{-1}) observed on 26 Jan 1993. The red and blue circles denote the edges of anticyclonic and cyclonic eddies, respectively.

oceanic anomalies are described in sections 3 and 4, respectively. The possible mechanisms for the decadal variation in ENSO–eddy relationship are discussed and analyzed in section 5. Section 6 summarizes the findings and implications from this study.

2. Data and methods

a. Datasets

In this study we used the sea level anomaly (SLA) and geostrophic current anomaly data from the Archiving, Validation, and Interpretation of Satellite Oceanographic Data (AVISO) mission to identify eddies in the SCS. The merged daily AVISO data are available from January 1993 to October 2014 and have a resolution of $1/4^\circ$ longitude \times $1/4^\circ$ latitude. The altimeter data contain aliases as a result of shelf, tidal, and internal waves over the shelf area (Yuan et al. 2006), which can introduce errors in eddy detection algorithms. Therefore, the SLA data in waters with depths shallower than 200 m are not used in this study. Also used are the monthly sea surface wind, sea surface temperature (SST), and sea level pressure (SLP) data during the period 1993–2014. The sea surface wind data are provided by a cross-calibrated multiplatform (CCMP) project that includes cross-calibrated satellite winds derived from a combination of many radar scatterometers (Atlas et al. 2011). The monthly CCMP wind product also has a resolution of $1/4^\circ$ longitude \times $1/4^\circ$ latitude. The monthly SST and SLP data are from the ERA-Interim of the European Centre for

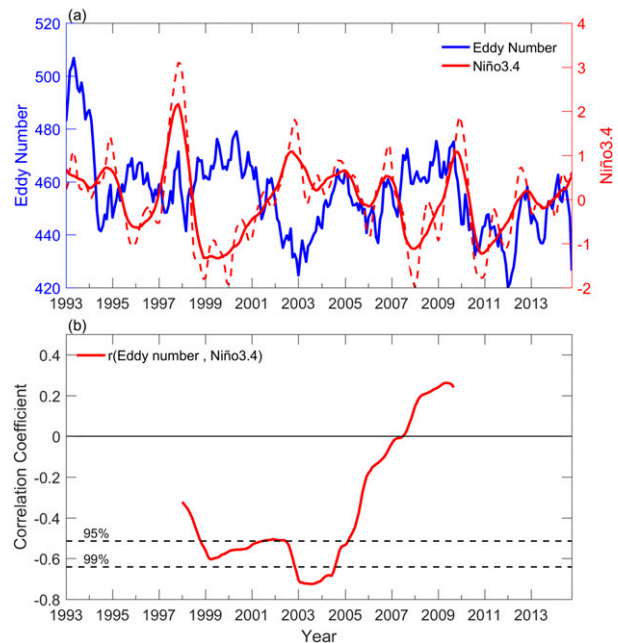


FIG. 2. (a) Monthly values of the number of mesoscale eddies in the SCS (solid blue) and Niño-3.4 index (dashed red), and (b) their 10-yr sliding correlations. Also shown are the Niño-3.4 index after an 11-month running mean has been applied (solid red) in (a), and the 95% and 99% significance levels of a Student's t test in (b).

Medium-Range Weather Forecasts, which has a resolution of $1/4^\circ$ longitude \times $1/4^\circ$ latitude (Dee et al. 2011). To calculate wind stress curl, we first used the bulk formulation of Trenberth et al. (1990) to calculate zonal and meridional components of wind stress τ_x and τ_y , respectively. We then applied Stokes's theorem to obtain the vertical component of $\text{curl}_z(\tau) = \nabla \times \tau$, which is the surface wind stress curl. To represent ENSO activity, we obtained the monthly Niño-3.4 index from the National Oceanic and Atmospheric Administration (NOAA). We also used the interdecadal Pacific oscillation (IPO) index from NOAA, and calculated the North Pacific Oscillation (NPO) index based on the previous study by Yu et al. (2012). Indices to represent the strengths of the northern and southern PMMs were also used in this study. Following Zhang et al. (2014), we calculated the monthly northern and southern PMM indices as the SST anomaly averaged over the northeast Pacific (21° – 25°N , 138° – 142°W) and the southeast Pacific (19° – 15°S , 103° – 107°W), respectively. Anomalies in this study are defined as the deviations from the climatological seasonal cycle for the period 1993–2014 after removing the linear trend.

b. Identification of mesoscale oceanic eddies

The GV method examines the geometry of velocity vectors to identify eddies (Nencioli et al. 2010). A mesoscale eddy is defined as a flow feature containing a

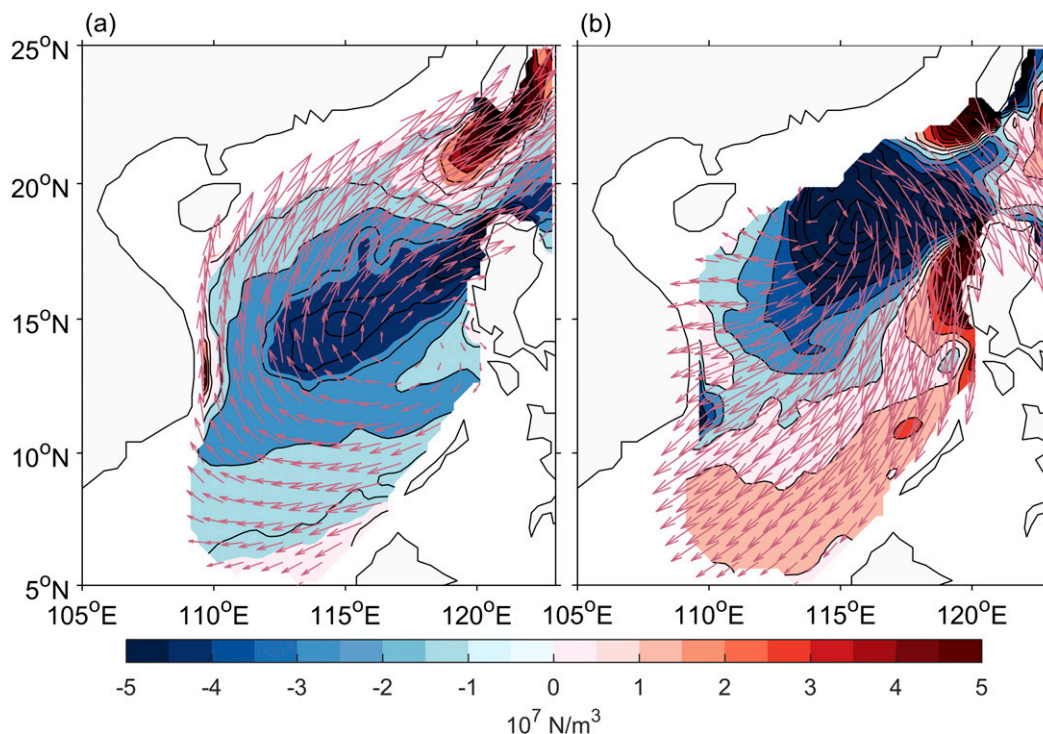


FIG. 3. The spatial patterns of the (a) EOF1 and (b) EOF2 modes of the wind stress curl anomalies (color and contour) over the SCS. Also shown are the regressions of surface wind anomalies (vector) onto (a) PC1 and (b) PC2.

consistent sense of rotation relative to a center of minimum speed and is surrounded by an enclosed streamline (as shown in Fig. 1). When applying the GV method to detect an eddy, there are two major steps in the calculation: one is to detect the eddy center and the other one is to determine the enclosed streamline that corresponds to the eddy center.

In searching for a potential eddy center, we need to localize the search area. Two parameters a and b are used to localize the search area and to set the minimum size of eddy detectable. Here the parameter a defines how many points away from a chosen center point will be examined, and the parameter b defines the horizontal size (in grid points) of the area used to calculate the local minimum velocity. Their values have to be tuned based on the data resolution to optimize the performance of the GV method (Nencioli et al. 2010). The performance can be assessed by the “success detection rate” ($\text{SDR} = N_c/N_i$) and the “excess detection rate” ($\text{EDR} = N_e/N_i$), where N_c is the number of eddies detected by both the expert and the detection method, N_i is the number of eddies identified by the expert only, and N_e is the number of eddies detected by the eddy detection method only. Because of the limited horizontal resolution of the altimeter data, only eddies with a radius larger than 25 km ($1/4^\circ$ grid) can be resolved.

Earlier studies have found that linearly interpolating the velocity field to higher-resolution grids can significantly improve the SDR and reduce the EDR (Liu et al. 2012; Lin et al. 2015; Xia and Shen 2015). To achieve the minimum size of eddy detectable standard while conserving computation resources, we choose to linearly interpolate the velocity field to a finer subgrid of $1/20^\circ \times 1/20^\circ$. This interpolation enables the minimum detectable radius to be reduced to 25 km. The parameter values used here ($a = 5$ and $b = 4$) are adapted from Xia and Shen (2015), who showed that these values produced the highest SDR and the lowest EDR when applying the GV method to the same AVISO dataset used in this study.

The outer edge of the eddy determined by the streamlines is calculated from the streamfunction ψ : $u' = -\partial\psi/\partial y$ and $v' = \partial\psi/\partial x$. Here, u' and v' are the zonal and meridional components of the sea surface geostrophic current anomaly, respectively. The edge of an eddy is defined as the outmost enclosed streamline around the eddy center provided that the velocity magnitudes from the enclosed streamline along an arbitrary radius to the eddy center decrease.

This GV method enables us to count the daily number of mesoscale eddies in the SCS. Figure 1 shows, as an example, the locations of anticyclonic eddies (AEs) and

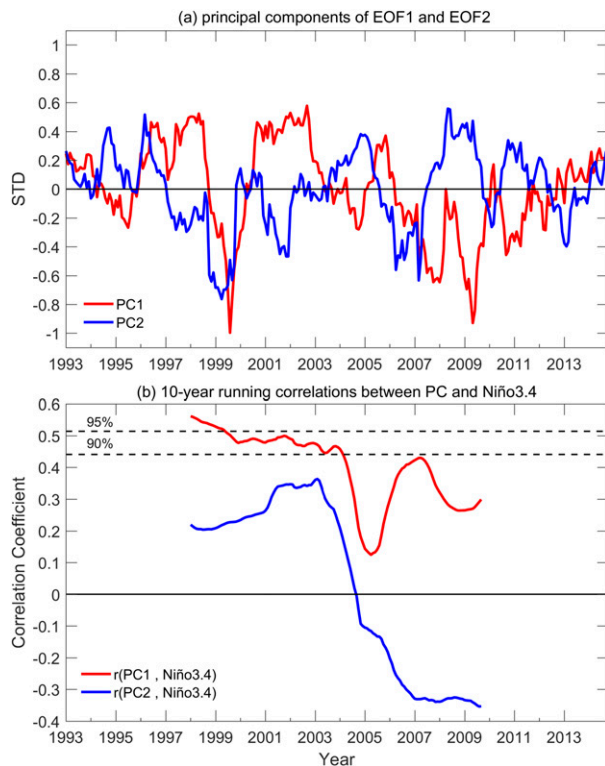


FIG. 4. (a) PC1 and PC2 of the first two EOF modes of wind stress curl anomalies over the SCS and (b) their 10-yr sliding correlations with the Niño-3.4 index. The PC values shown are normalized by their standard deviations and have been applied with an 11-month running mean. The 90% and 95% significance levels are marked in (b).

cyclonic eddies (CEs) identified by the GV method for 26 January 1993. On this particular day, there are a total of 15 mesoscale eddies in the SCS, which includes 9 CEs and 6 AEs. The eddies on this day are distributed more or less evenly across the SCS basin, which is in general consistent with mean climatology of eddy probability reported in earlier studies (e.g., Chen et al. 2011). It should be noted here that only SLA differences larger than 2 cm can be observed accurately by the satellite (Pujol et al. 2016). To avoid errors introduced by the observations, we omitted any eddy with an amplitude smaller than 2 cm from our results (e.g., the two AEs off Hainan in Fig. 1).

3. Relationships between ENSO and SCS mesoscale eddies

We examine the eddy–ENSO relationship first by showing in Fig. 2a the time series of the monthly values of the eddy number in the SCS and the Niño-3.4 SST index. The monthly values of the eddy number were calculated as the sum of the daily eddy number identified by the GV method and ranged between 400 and 500

eddies (per month) during 1993–2014. The immediate impression from the figure is that there is a tendency for the eddy number to be out of phase with the Niño-3.4 index. This indicates that the eddy number in the SCS decreases during El Niño events but increases during La Niña events. This negative ENSO–eddy relationship is consistent with the findings of some previous studies (e.g., Cheng and Qi 2010; Chen et al. 2011; He et al. 2016; Chu et al. 2017). We have also used three other identification methods—that is, the SLA-based method (Wang et al. 2003), the Okubo–Weiss (OW) approach method (Okubo 1970; Weiss 1991), and the hybrid (HY) method (Yi et al. 2014)—to calculate the mesoscale eddy number in the SCS and then to recalculate the ENSO–eddy relationship; the results obtained (not shown) are similar to those in Fig. 2b.

However, the correlation does not seem to be stationary throughout the entire analysis period. In particular, the out-of-phase relationship becomes less evident after 2004. This initial analysis indicates that there may be a change in the ENSO–eddy relationship around 2004. To confirm this and to more precisely determine the timing of the change, we show in Fig. 2b a sliding correlation between the eddy number and the Niño-3.4 index using a 10-yr moving window. This figure confirms that the ENSO–eddy relationship changed around 2004 from being significantly and negatively correlated before to noncorrelated afterward. The eddy number shows a stronger negative correlation with the Niño-3.4 index that passes the 95% significance level only during the pre-2004 era. Therefore, in the rest of this study we focus on understanding how the ENSO–eddy relationships are established before and after 2004.

Surface wind stress curl is one of the most relevant generation mechanisms for mesoscale oceanic eddies and needs to be analyzed in order to understand the ENSO–eddy relationships. To identify the leading modes of variation in surface wind stress curl over the SCS, we perform an empirical orthogonal function (EOF) analysis to the curl anomalies over the SCS (5° – 25° N, 105° – 123° E). The two leading EOF modes (EOF1 and EOF2) explain 21.3% and 12.8%, respectively, of the total variance and distinguish themselves from the rest of the EOF modes (not shown). Therefore, we focus only on these two modes.

The spatial pattern of EOF1 (Fig. 3a) consists of a basin-scale monopole of wind stress curl anomalies with an elongated band extending from the center (15° N, 115° E) of the analysis box toward a region to the northwest of Luzon Island. In its positive phase, EOF1 is characterized by an anomalous anticyclone covering almost the entire SCS basin. This wind stress curl pattern can spin down the gyre-scale circulation in the SCS,

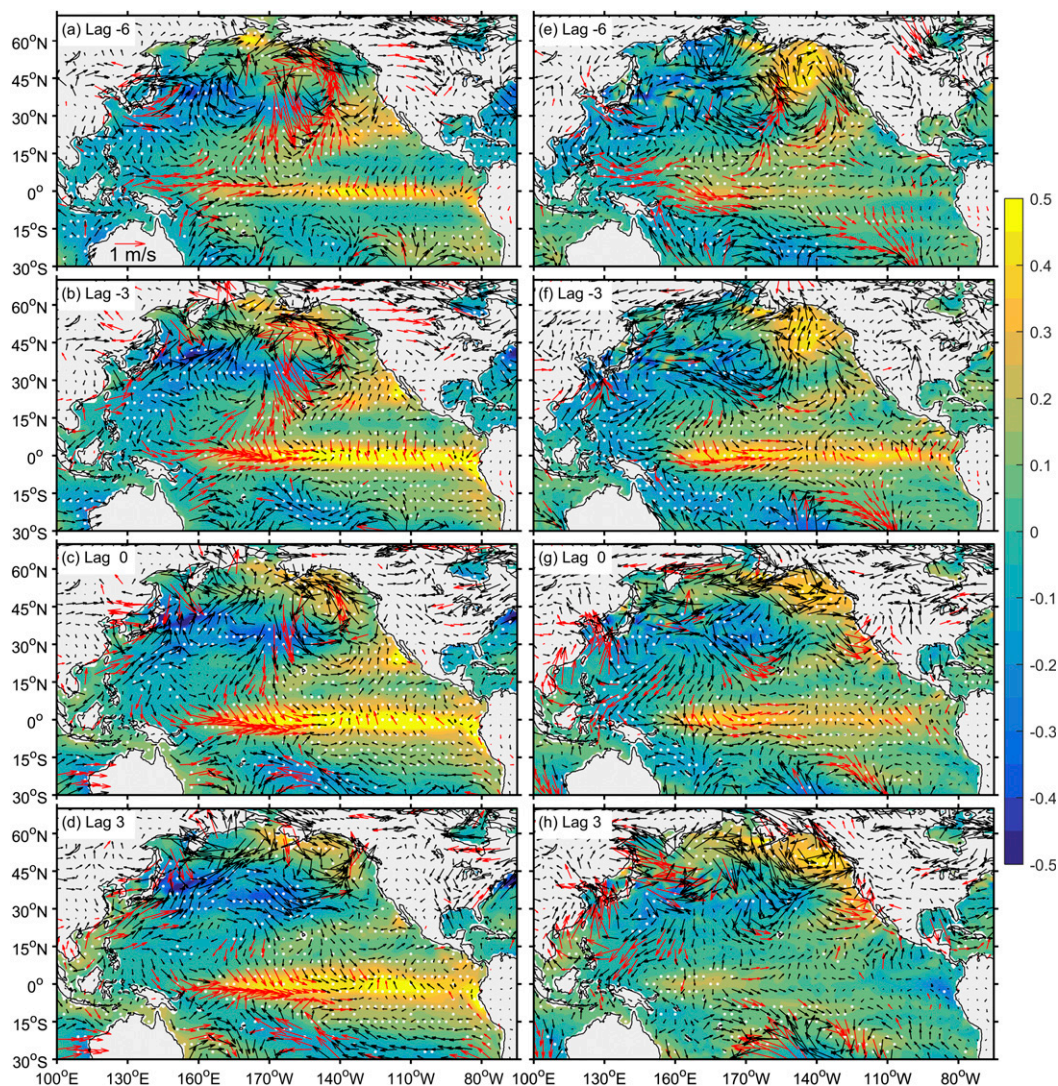


FIG. 5. Lead-lagged regressions of SST (color; $^{\circ}\text{C}$) and sea surface wind anomalies (vectors; m s^{-1}) onto PC1 during (a)–(d) P1 and (e)–(h) P2, and onto PC2 during (i)–(l) P1 and (m)–(p) P2. The lag values (months) are shown at the left top of each panel. The white dots and red vectors indicate regressions that exceed the 90% significance level, based on a Student's t test.

which is cyclonic over the entire SCS during boreal winter (Fang et al. 2006; Y. Wang et al. 2006; Cheng and Qi 2010) and cyclonic north of 12°N during boreal summer (Fang et al. 2006; G. Wang et al. 2008). Therefore, the EOF1 pattern (in its positive phase) can weaken the SCS gyre-scale circulation and its associated baroclinic instability, resulting in a reduction in the mesoscale eddy activity in the SCS. As for EOF2 (Fig. 3b), its spatial pattern exhibits a meridional dipole of wind stress curl anomalies with a slight northwest-to-southeast tilt. The northwest lobe of the dipole is located to the east of Hainan Island, while the southeast lobe is located to the west of Luzon Island. Associated with this anomalous curl pattern, an anticyclonic wind stress anomaly pattern

occupies most of the SCS. The negative wind stress curl anomalies are stronger and occupy most of the SCS, especially north of 12°N , while the positive wind stress curl anomalies are weaker and occupy the regions to the south. This EOF pattern (in its positive phase) can spin down the summer gyre-scale circulation and a large part of the winter gyre-scale circulation, resulting in a weakening of SCS mesoscale eddy activity during both seasons. These two EOF patterns can also affect the SCS eddy activity by modulating the Kuroshio intrusion, which is another major generation mechanism for the mesoscale eddies in the SCS (Metzger and Hurlburt 2001; Jia and Chassignet 2011; Nof et al. 2011). In their positive phase, both EOF1 and EOF2 have positive wind stress curl

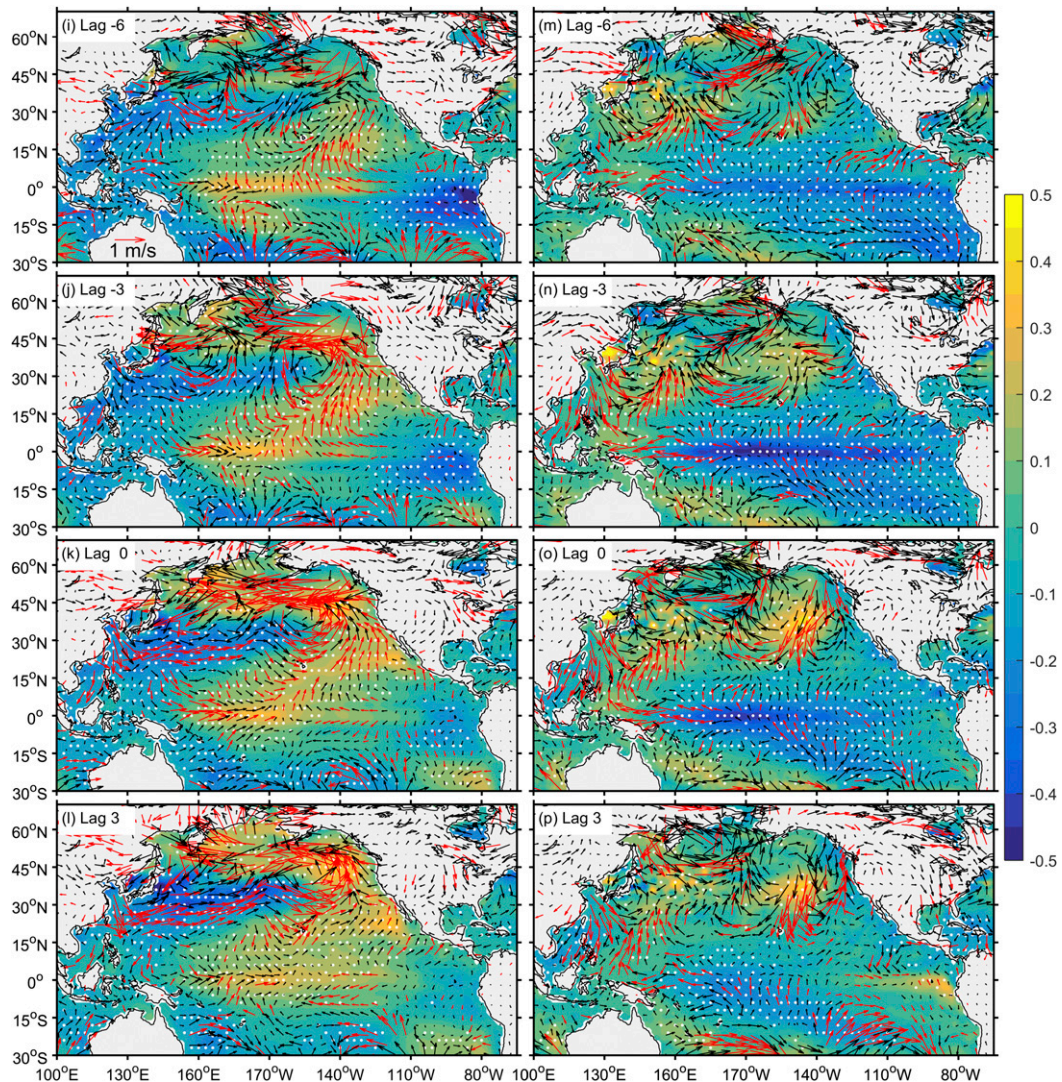


FIG. 5. (Continued)

anomalies southwest of Taiwan that lower local sea surface heights through Ekman transport and negative wind stress curl anomalies northwest of Luzon that elevate local sea surface heights (Metzger and Hurlburt 2001; Liang et al. 2008; Hsin et al. 2012; Wu and Hsin 2012). The resulting meridional pressure gradient across the Luzon Strait can weaken the Kuroshio intrusion into the SCS (Qu 2000; Metzger and Hurlburt 2001; Liang et al. 2008; Hsin et al. 2012; Wu and Hsin 2012), reducing mesoscale eddy activity in the SCS. Therefore, both the EOF1 and EOF2 modes tend to reduce (increase) eddy production over a large part of the SCS by influencing the SCS gyre-scale circulation and Kuroshio intrusions during their positive (negative) phase.

We next examine how these two leading modes are related to ENSO. Figure 4 shows the principal components

of these two EOFs (i.e., PC1 and PC2) and their 10-yr sliding correlation with the Niño-3.4 index. As shown in Fig. 4b, it is interesting to find that these two modes show similar positive correlations with Niño-3.4 index before 2004 but dramatically opposite correlations with Niño-3.4 index after 2004. The EOF1 mode of wind stress curl anomalies maintains its positive correlation with the Niño-3.4 index throughout the analysis period, but the EOF2 mode changes from being positively correlated with Niño-3.4 index before 2004 to negatively correlated afterward. Therefore, these two EOF modes respond similarly to ENSO before 2004 to enable El Niño (La Niña) to weaken (strengthen) the production of SCS mesoscale eddies, but they respond opposite after 2004 to cancel each other out, resulting in a weak relationship between SCS eddies and ENSO. The change in the correlation seen in Fig. 2b

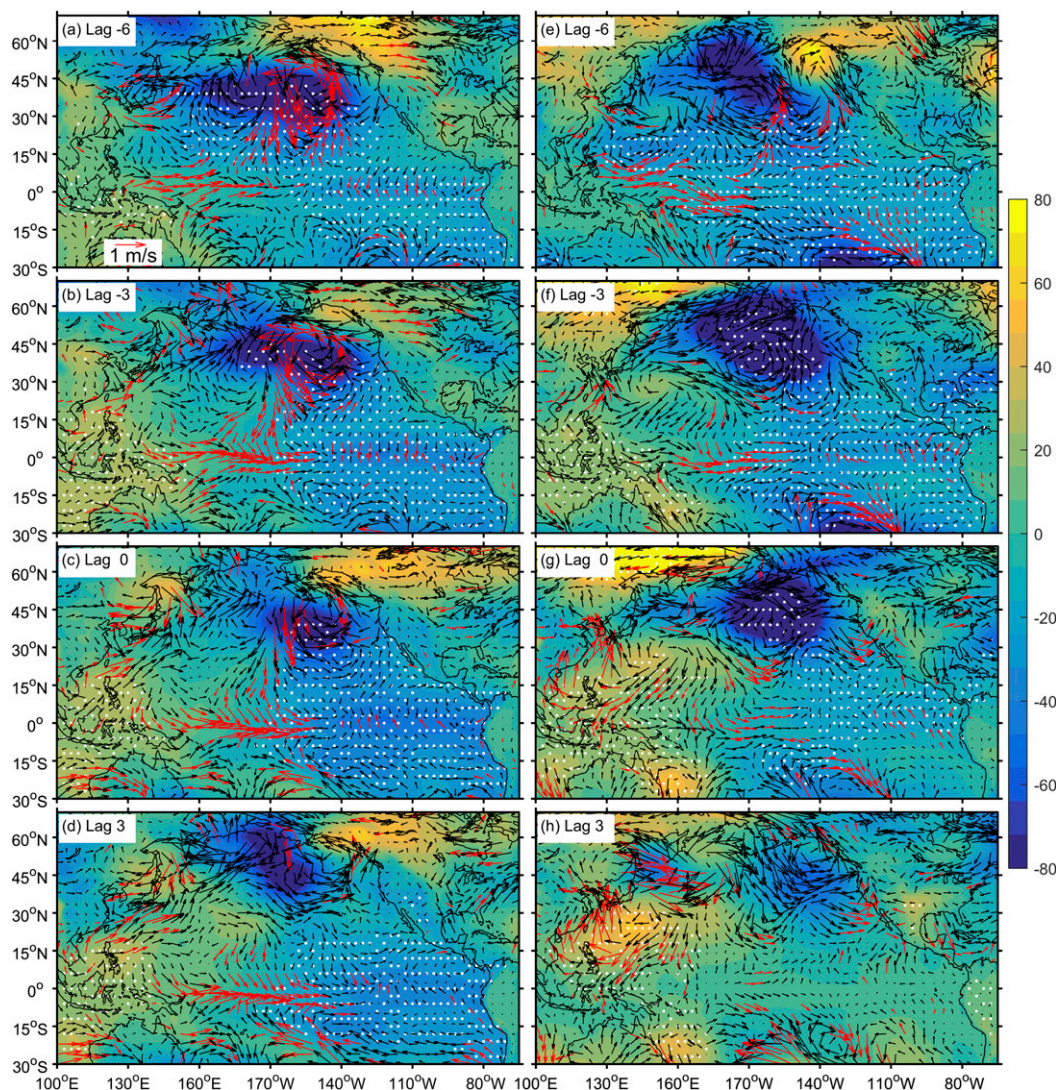


FIG. 6. As in Fig. 5, but for the regressions of SLP (color and shading; Pa) and sea surface wind (vector; m s^{-1}) anomalies.

between ENSO and the SCS eddy number around 2004 can be a result from the enhancement and cancelation between these two EOF modes before and after that time, respectively.

4. Large-scale atmospheric and oceanic anomalies associated with modes of SCS wind stress curl variability

We then examine the large-scale atmospheric circulation and SST anomalies associated with these two leading modes by regressing SST, SLP, and surface wind anomalies onto PC1 and PC2 during the period before 2004 (1993–2003; P1) and the period afterward (2004–14; P2). Both of the SST regressions onto PC1 during P1

(Figs. 5a–d) and P2 (Figs. 5e–h) are dominated by a typical evolution of El Niño (Rasmusson and Carpenter 1982). The SST anomalies originate first off the South American coast and spread westward along the equatorial Pacific. The regressions of SLP onto PC1 (Figs. 6a, d, e–h) also reveal several typical features associated with a developing ENSO event. One of them is the Southern Oscillation pattern over the tropical Pacific that is characterized by negative SLP anomalies over the tropical eastern Pacific and positive SLP anomalies over the tropical western Pacific. When we zoom into the lag 0 regressions around the SCS region (Figs. 7a,b), we can clearly see that the positive SLP anomalies over the SCS are part of the western Pacific center of the Southern Oscillation during both P1 and P2 (cf. Figs. 7a,b, 6c,g).

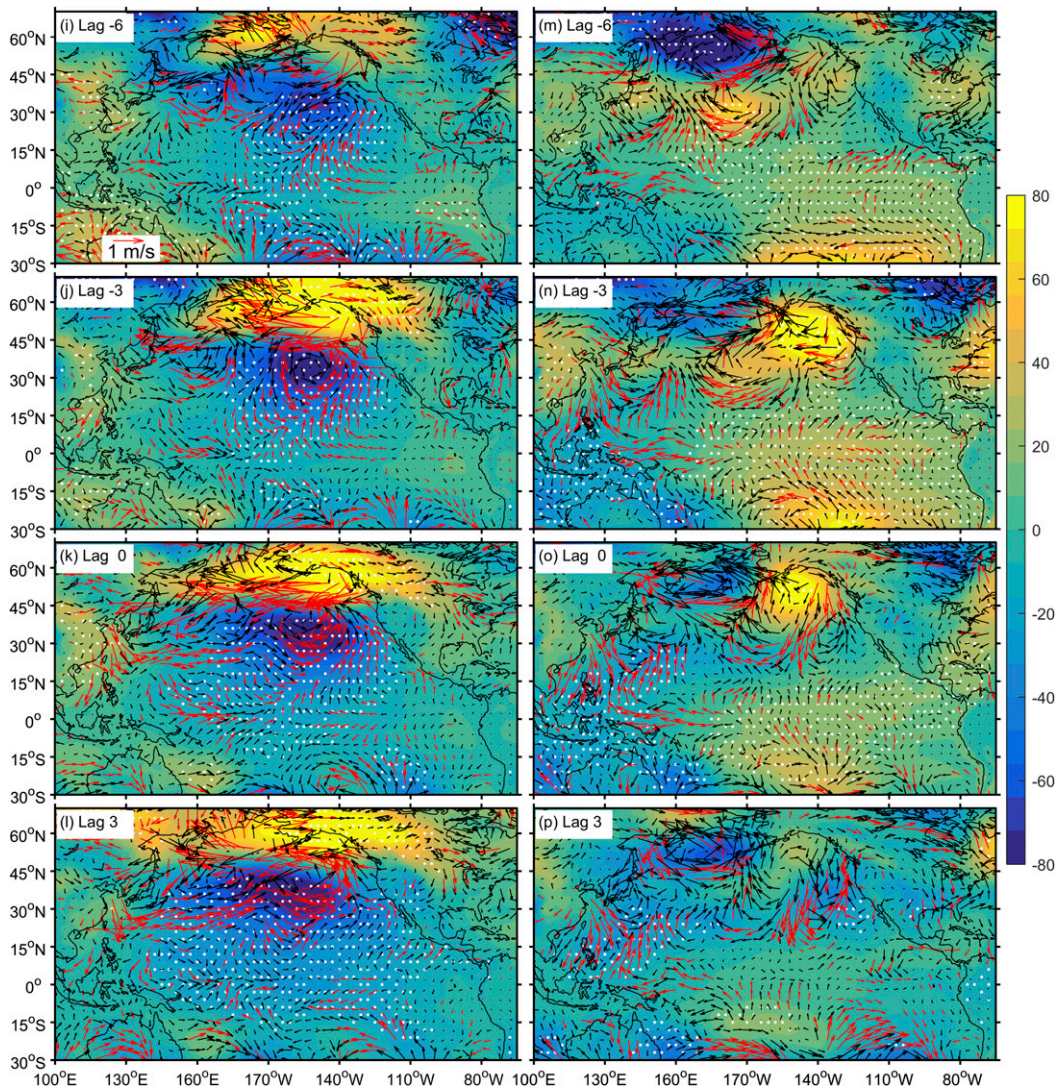


FIG. 6. (Continued)

The positive SLP anomalies over the SCS have a local center over the Philippine Sea that induces an anticyclonic wind stress pattern over the entire SCS that resembles the EOF1 mode (cf. Figs. 7a,b, 3a). These regression analyses indicate that the EOF1 mode of wind stress curl variations over the SCS is part of the Southern Oscillation that accompanies the developing ENSO during both P1 and P2. This explains why the EOF1 mode maintains a stationary positive correlation with the Niño-3.4 index throughout the analysis period.

As mentioned above, the EOF2 mode exhibits a remarkable change in its relationship with the Niño-3.4 index around 2004. During the pre-2004 period (i.e., P1), the SST regression (Figs. 5i–l) is dominated by a pattern like the northern Pacific meridional mode (nPMM) (Chiang and Vimont 2004) that features warm SST

anomalies spreading from the North American coast to the tropical central Pacific and cool SST anomalies that persist in the tropical eastern Pacific. After PC2 and the nPMM reaches their peak phases at lag 0, the warm SST anomalies at the tropical central Pacific continue to develop into an El Niño event. This El Niño resembles more closely the central Pacific El Niño (Yu and Kao 2007; Kao and Yu 2009) than the conventional eastern Pacific El Niño. This is consistent with the suggestion that the nPMM is a precursor of ENSO (e.g., Chang et al. 2007; Yu et al. 2010; Yu and Kim 2011; Yu et al. 2017). As such, PC2 leads the development of El Niño; this is in contrast to PC1, which develops together with El Niño. Therefore, the EOF2 mode of the surface wind stress curl variations in the SCS is associated with a precursor of ENSO before 2004 (i.e., during P1). The

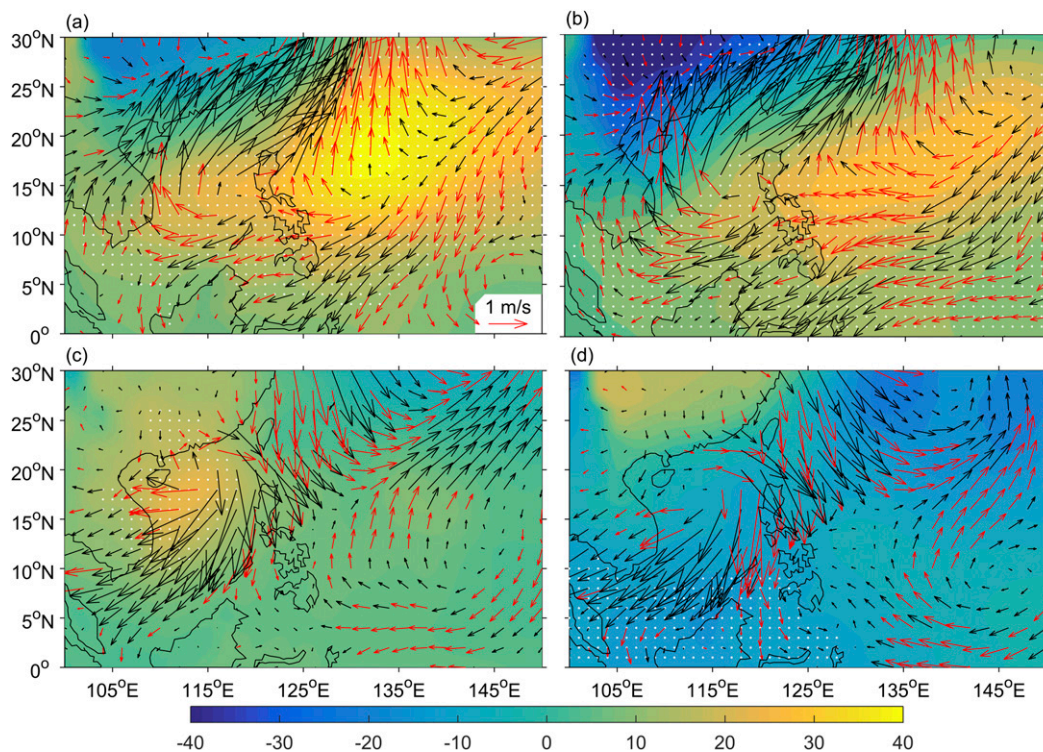


FIG. 7. SLP (color and contour; Pa) and surface wind (vector; m s^{-1}) anomalies in the SCS regressed onto the (a),(b) PC1 index and (c),(d) PC2 index during subperiods (left) P1 and (right) P2. The white dots and red vectors indicate regressions that exceed the 90% significance level, based on a Student's test.

positive correlation between PC2 and the Niño-3.4 index in Fig. 4c during this subperiod does not represent an SCS response to El Niño but rather a joint connection of the EOF2 and ENSO with the nPMM. We show in Fig. 8 the lead-lag correlations between the two PCs and the Niño-3.4, nPMM, and southern PMM (sPMM) indices for the two periods (P1 and P2). The figure shows that PC2 has a larger simultaneous (lag 0) correlation coefficient with the nPMM index (0.37) than with the Niño-3.4 index (0.08) during the P1 subperiod (Fig. 8c). In contrast, PC1 has a larger simultaneous correlation with the Niño-3.4 index (0.37) during this period. Our analyses indicate that the negative correlation between the SCS eddy activity and ENSO can be established directly through ENSO (i.e., the EOF1 mode) and indirectly through an ENSO precursor—the northern PMM (i.e., the EOF2 mode) before 2004.

The SLP regression onto PC2 during the pre-2004 period (Figs. 6i–l) is dominated by an NPO pattern (Walker and Bliss 1932; Rogers 1981; Linkin and Nigam 2008), which is characterized by an out-of-phase variation between the Aleutian low and the Pacific subtropical high. The correlation coefficient between PC2 and the NPO index is 0.75 during P1. Recent studies have suggested that the NPO can induce SST anomalies

off Baja California via anomalous surface heat fluxes, which then spread southwestward via subtropical Pacific atmosphere–ocean coupling into the equatorial Pacific to trigger the development of ENSO in the tropical central Pacific (Kao and Yu 2009; Yu et al. 2010; Yu and Kim 2013; Yu et al. 2017). This sequence of events is similar to those associated with the positive nPMM pattern and the ENSO onset shown in Figs. 5i–l. The regressed surface wind anomalies (particularly at lag 0; Figs. 5k, 6k) show that an anomalous surface cyclone forms over the western North Pacific (covering the region from Japan to Taiwan) in association with the nPMM. This cyclonic anomaly is a Gill-type response to the positive SST anomalies associated with the nPMM that has been mentioned in previous studies of the PMM (e.g., Wang et al. 2012; Zhang et al. 2016). This anomalous cyclonic circulation induces anomalous northerly winds over the SCS similar to those in the EOF2 pattern (cf. Figs. 7c, 3b).

During the post-2004 period (i.e., P2), the SST regression onto PC2 (Figs. 5m–p) is very different from that obtained during the pre-2004 period. The regressed anomalies are dominated by an sPMM (Zhang et al. 2014) in the southeastern Pacific. The sPMM is the Southern Hemispheric analog of the nPMM and is

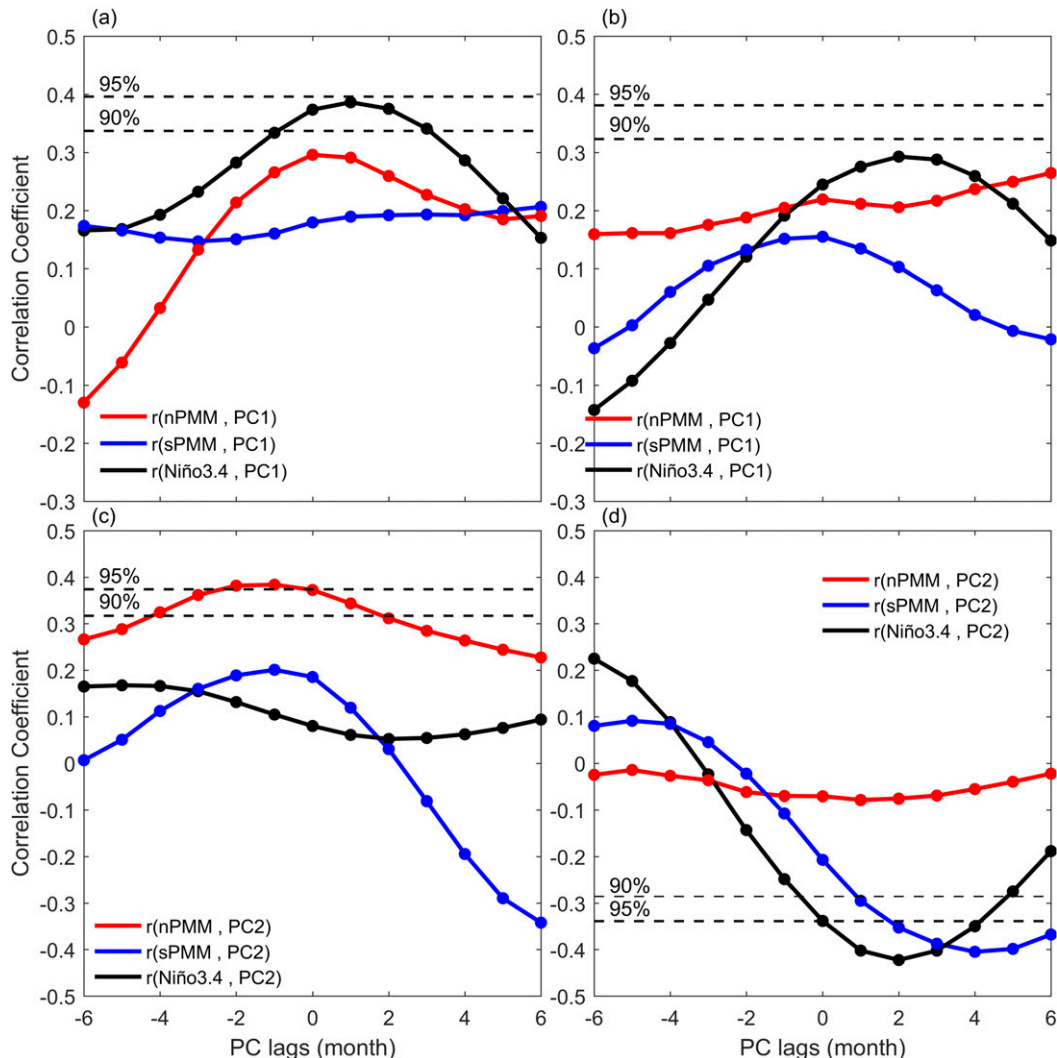


FIG. 8. (a),(b) Lead-lag correlation between 5-month running mean PC1 and the Niño-3.4, northern and southern PMM indices during subperiods (left) P1 and (right) P2. (c),(d) As in (a) and (b), respectively, but for PC2. The 90% and 95% significance levels of a Student's t test are marked.

characterized by SST anomalies extending from the Peruvian coast toward the equatorial central Pacific. As shown in Fig. 8d, PC2 has a larger simultaneous correlation coefficient with the sPMM index (-0.22) than with the nPMM index (-0.07) during the P2 subperiod. The sPMM is capable of developing into the deep tropics through its connection with cold tongue ocean dynamics (e.g., mean advection) (Zhang et al. 2014). As shown in Figs. 5m–p, cold SST anomalies developed at the equator together with the evolution of the negative phase of the sPMM. As a result, PC2 also shows a large negative correlation with the Niño-3.4 index during this period. It should be noted that the positive values of the PC2 are associated with a “cold” phase of the sPMM and a La Niña during P2 but associated with a “warm” phase of the nPMM and an El Niño during P1. This

explains why the correlation between PC2 and the Niño-3.4 index changed from positive before 2004 to negative afterward. The SLP anomalies regressed onto PC2 during P2 (Figs. 6m–p) are dominated by positive values over the southeastern Pacific, a typical pattern associated with the cold sPMM pattern [cf. Fig. 1f of Zhang et al. (2014)]. The regressed surface wind anomalies indicate an anomalous anticyclonic circulation formed between 130°E and 180° as a Gill-type response to the cold SST anomalies associated with the sPMM (Figs. 5o, 6o). As part of a Rossby wave response, an anomalous cyclonic circulation forms farther to the west over the western North Pacific. The anomalous cyclone extends from Japan into the Philippine Sea and induces an anomalous northerly pattern in the SCS that is similar to the EOF2 mode. This similarity can be better seen by

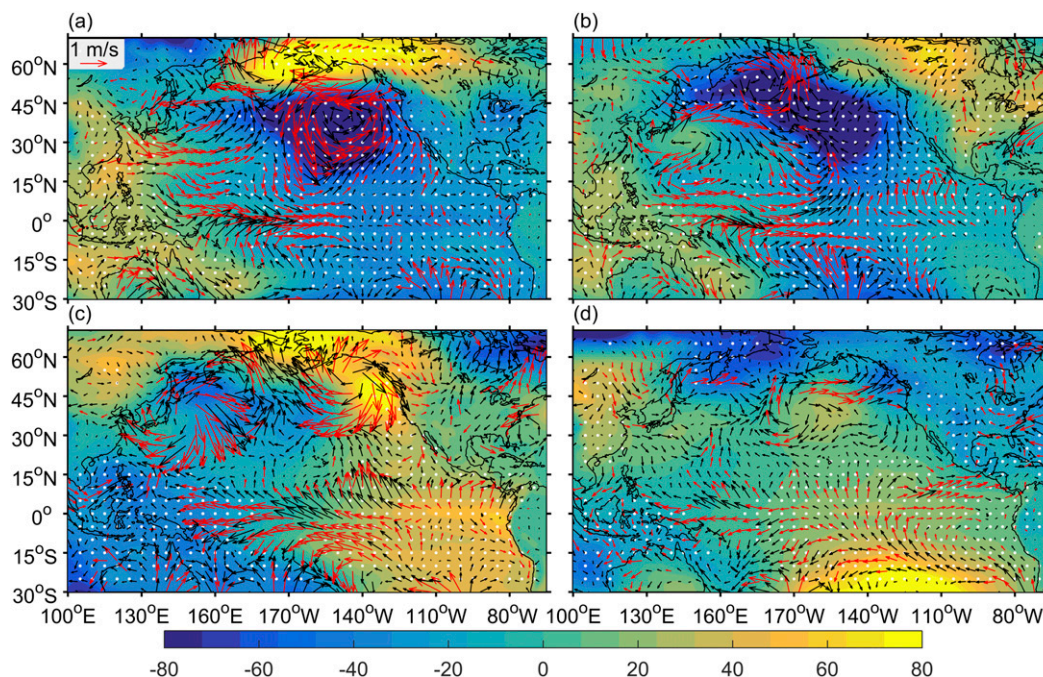


FIG. 9. SLP (color; Pa) and surface wind anomalies (vectors; m s^{-1}) regressed onto (a),(b) the nPMM index and (c),(d) the sPMM index (sign reversed, see text) during subperiods (left) P1 and (right) P2. The white dots and red vectors indicate regressions that exceed the 90% significance level, based on a Student's test.

focusing on the anomalies around the SCS (Fig. 7d). It is very interesting to find that a similar wind stress anomaly pattern in the SCS can be produced as a direct Gill-type response to the nPMM during P1 or as part of a Rossby wave train associated with the Gill-type response to the sPMM during P2.

To further confirm that EOF2 is indeed related to the nPMM before 2004 (i.e., P1) but to the sPMM afterward (i.e., P2), we show in Fig. 9 the wind and SLP anomaly patterns regressed onto the nPMM and sPMM indices during the two subperiods. The figure shows that during P1, the nPMM-regressed wind and SLP anomaly patterns are similar to those regressed onto the PC2 during P1 (cf. Figs. 6k, 9a), with a pattern correlation coefficient of 0.76. In both sets of regressions, surface northerlies prevail south of 12°N throughout the SCS. However, the nPMM regressions during P2 are very different from the PC2 regressions during that period (cf. Figs. 6g, 9b), with a pattern correlation coefficient between them of only -0.23 . Besides having a very different SLP anomaly pattern from the PC2 regressions, the nPMM regressions show very weak surface wind anomalies over the SCS during this period. In contrast, sPMM-regressed wind and SLP anomaly are similar to those regressed onto PC2 during P2 (cf. Figs. 6g, 9d) but not during P1 (cf. Figs. 6k, 9c). Their pattern correlations reach 0.42 during P2 but only 0.22 during P1. Since the positive phase of EOF2 is related to the negative phase of the

sPMM, the signs of the regression patterns in Figs. 9c and 9d have been reversed to aid the comparison with Figs. 6g and 6k. The sPMM regressions show prevailing northerlies throughout the entire SCS during P2 but only to the north of 12°N during P1.

Thus, our analyses suggest that the EOF1 mode of wind stress curl variations in the SCS is directly forced by ENSO via the Southern Oscillation throughout the analysis period, whereas the EOF2 pattern is forced by the nPMM before 2004 and by the sPMM after 2004. Also, the nPMM links the positive phase of the EOF2 to El Niño, while the sPMM links the positive EOF2 to La Niña. As a result, when an El Niño event occurred during the pre-2004 period, it was associated with a positive phase of EOF1 and a positive phase of the EOF2 that together produce anticyclonic wind stress curl anomalies over the SCS. This weakened wind stress curl thus curbed the production of mesoscale eddies in the SCS. In contrast, when an El Niño event occurred during the post-2004 period, it was associated with a positive phase of the EOF1 and a negative phase of the EOF2, and the wind stress curl anomalies over the SCS tended to be weak as a result and so there was a weak ENSO impact on SCS eddy activity during this subperiod. The differing relationship between the SCS eddy number and the ENSO before and after 2004 is caused by the differing associations of the EOF2 mode with the northern and southern PMMs around that time. To further confirm the changed relationships between the

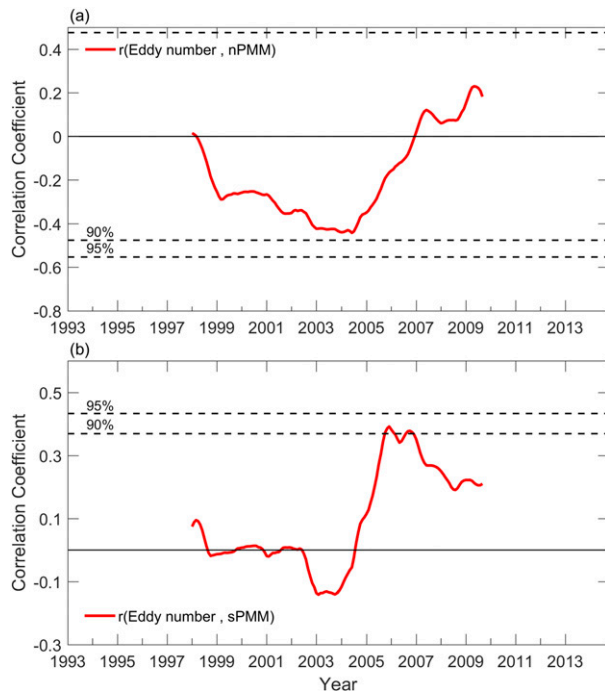


FIG. 10. (a) The 10-yr sliding correlations between the eddy number anomaly in the SCS and the nPMM. (b) As in (a), but for the sPMM. Also shown are the 90% and 95% significance levels of a Student t test in (a) and (b).

SCS eddy number and the two PMMs, we show in Fig. 10 the 10-yr sliding correlations between the monthly eddy number anomaly and the nPMM and sPMM indices. This figure clearly shows that the SCS eddy number was more strongly correlated with the nPMM during the period before 2004 but more correlated with the sPMM afterward. This result adds support to our finding on the relative importance of the northern and southern PMMs for the SCS eddy activity changes from decade to decade.

5. Influences of the IPO on the recent ENSO–eddy relation changes

A key question to ask is what causes the EOF2–PMM relation to change around 2004? We notice that 2004 is close to the time when the IPO switches from its positive to negative phase (Fig. 11). The IPO’s phase change may be the reason for the change in EOF2–PMM relations around 2004. The SST and SLP anomalies regressed onto the IPO index during the subperiods before and after 2004 are shown in Fig. 12. It shows that the ENSO-like SST variability associated with the IPO (Figs. 12a,c) is associated with large SLP anomalies over both the northeastern and southeastern Pacific (Figs. 12b,d) during both periods. These are the regions where the nPMM and sPMM are located. The figure indicates that

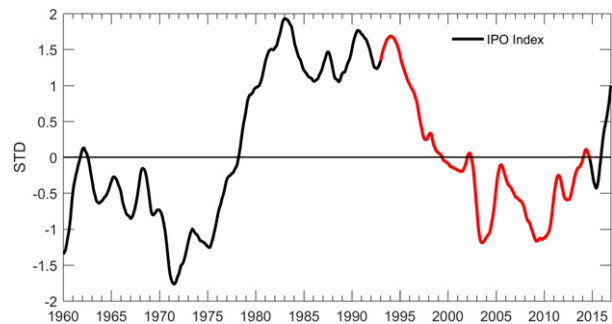


FIG. 11. The IPO index after a 10-yr running mean (standard deviation). The red part marks the analysis period of this study.

SLP anomalies over the sPMM region increased in magnitude from P1 to P2. Figure 12 suggests that the SLP anomalies produced by the IPO change the strengths of the background trade winds in these two regions, resulting in a difference in the relative importance of the nPMM and sPMM before and after 2004. This possible modulation effect of the IPO on the nPMM and sPMM requires a more extensive study of the northern and southern PMM dynamics that is beyond the scope of this study.

6. Summary and discussion

In this study we have examined the interannual variability in the number of mesoscale eddies in the SCS and its relationship with ENSO. While previous studies have already provided useful findings on the impact of ENSO on SCS eddies, our research uncovered a change in the ENSO influence in recent years, specifically around 2004. Furthermore, we find that the ENSO–eddy relationship is controlled by two wind stress curl mechanisms: one directly related to ENSO and the other related to precursors of ENSO—the northern and southern PMMs.

These two mechanisms appear as the two leading EOF modes of the interannual variability in surface wind stress curl over the SCS. While the direct ENSO mechanism produces a negative ENSO–eddy correlation throughout the analysis period, the indirect PMM mechanism produces a negative ENSO–eddy correlation before 2004 but a positive ENSO–eddy correlation afterward. As a result, ENSO can strongly impact the number of SCS eddies through the additive effects of both ENSO and ENSO-precursor (i.e., the PMMs) mechanisms before 2004, but it has little impact on the SCS eddy number after 2004 as a result of the cancellation between these two mechanisms. The differing ENSO–eddy correlation produced by the PMM mechanism may be related to a phase change of the IPO around 2004, which links the SCS eddies to the northern

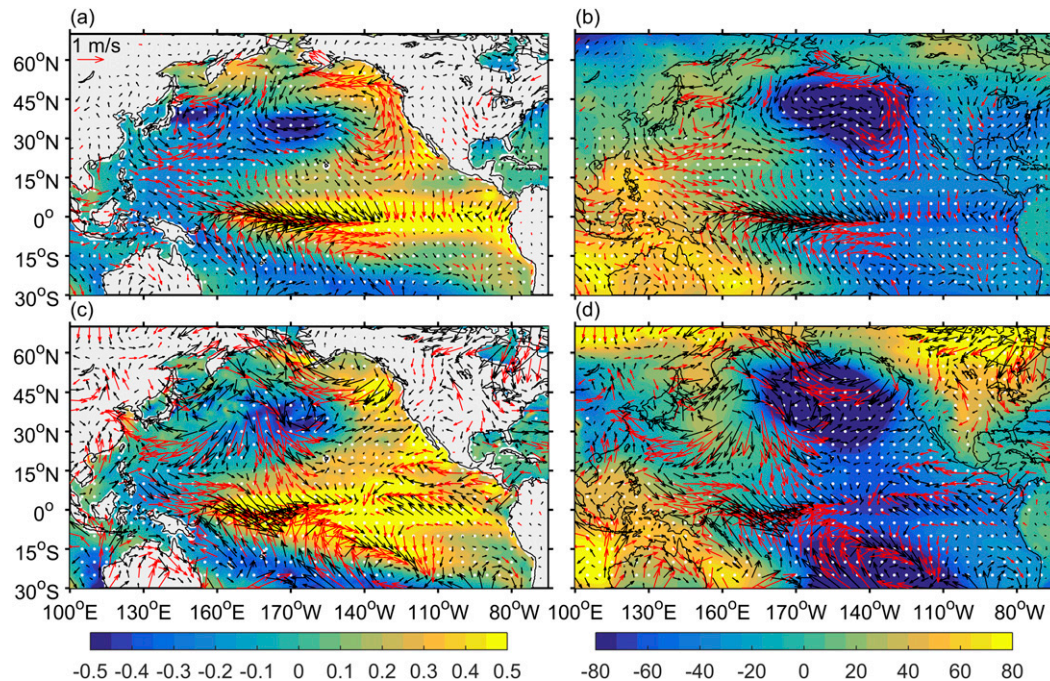


FIG. 12. Regressions of (left) SST ($^{\circ}\text{C}$) and (right) SLP (Pa) anomalies onto the IPO index during the (top) P1 and (bottom) P2 subperiods. The regressions of surface wind (vector; m s^{-1}) anomalies are superimposed in all panels. The white dots and red vectors indicate regressions that exceed the 90% significance level, based on a Student's t test.

PMM during the pre-2004 period but to the southern PMM during the post-2004 period.

One major finding of this study is that both the northern and southern PMMs can produce strong impacts on mesoscale oceanic eddies in the SCS, which has not been documented previously. While the northern PMM has been extensively studied, the southern PMM has not received the same attention. Much is still unknown about why and how the relative importance of these two PMMs can be modulated by the phase change of the IPO and what that implies for decadal changes in SCS eddy activities. These issues were not addressed in this study and require further investigations. It should be noted that the findings reported here are based on datasets that are rather short for a study of interannual and (especially) interdecadal variability as a result of the limited availability of altimetry observations in the SCS. We suggest that the analyses presented here should be repeated when longer periods of data become available to verify our findings.

Acknowledgments. We thank three anonymous reviewers for their valuable comments. We thank the European Centre for Medium-Range Weather Forecasts, Remote Sensing Systems, and AVISO for making the datasets used in this study available online. Pengfei Tuo and Jianyu Hu were supported by the National Natural Science Foundation of China (41776027) and the National

Basic Research Program of China (2015CB954004). Jin-Yi Yu was supported by the National Science Foundation's Climate and Large-Scale Dynamics Program under Grants AGS-1505145 and AGS-1833075. Pengfei Tuo was also supported by the China Scholarship Council (201606310171).

REFERENCES

- Atlas, R., R. N. Hoffman, J. Ardizzone, S. M. Leidner, J. C. Jusem, D. K. Smith, and D. Gombos, 2011: A cross-calibrated, multiplatform ocean surface wind velocity product for meteorological and oceanographic applications. *Bull. Amer. Meteor. Soc.*, **92**, 157–174, <https://doi.org/10.1175/2010BAMS2946.1>.
- Chang, P., L. Zhang, R. Saravanan, D. J. Vimont, J. C. Chiang, L. Ji, H. Seidel, and M. K. Tippett, 2007: Pacific meridional mode and El Niño–Southern Oscillation. *Geophys. Res. Lett.*, **34**, L16608, <https://doi.org/10.1029/2007GL030302>.
- Chao, S. Y., P. T. Shaw, and S. Y. Wu, 1996: El Niño modulation of the South China Sea circulation. *Prog. Oceanogr.*, **38**, 51–93, [https://doi.org/10.1016/S0079-6611\(96\)00010-9](https://doi.org/10.1016/S0079-6611(96)00010-9).
- Chen, G., Y. Hou, Q. Zhang, and X. Chu, 2010: The eddy pair off eastern Vietnam: Interannual variability and impact on thermohaline structure. *Cont. Shelf Res.*, **30**, 715–723, <https://doi.org/10.1016/j.csr.2009.11.013>.
- , —, and X. Chu, 2011: Mesoscale eddies in the South China Sea: Mean properties, spatiotemporal variability, and impact on thermohaline structure. *J. Geophys. Res.*, **116**, C06018, <https://doi.org/10.1029/2010JC006716>.
- Cheng, X., and Y. Qi, 2010: Variations of eddy kinetic energy in the South China Sea. *J. Oceanogr.*, **66**, 85–94, <https://doi.org/10.1007/s10872-010-0007-y>.

- Chi, P. C., Y. Chen, and S. Lu, 1998: Wind-driven South China Sea deep basin warm-core/cool-core eddies. *J. Oceanogr.*, **54**, 347–360, <https://doi.org/10.1007/BF02742619>.
- Chiang, J. C., and D. J. Vimont, 2004: Analogous Pacific and Atlantic meridional modes of tropical atmosphere–ocean variability. *J. Climate*, **17**, 4143–4158, <https://doi.org/10.1175/JCLI4953.1>.
- Chu, P. C., N. L. Edmons, and C. Fan, 1999: Dynamical mechanisms for the South China Sea seasonal circulation and thermohaline variabilities. *J. Phys. Oceanogr.*, **29**, 2971–2989, [https://doi.org/10.1175/1520-0485\(1999\)029<2971:DMFTSC>2.0.CO;2](https://doi.org/10.1175/1520-0485(1999)029<2971:DMFTSC>2.0.CO;2).
- Chu, X., C. Dong, and Y. Qi, 2017: The influence of ENSO on an oceanic eddy pair in the South China Sea. *J. Geophys. Res. Oceans*, **122**, 1643–1652, <https://doi.org/10.1002/2016JC012642>.
- Dee, D. P., and Coauthors, 2011: The ERA-Interim reanalysis: Configuration and performance of the data assimilation system. *Quart. J. Roy. Meteor. Soc.*, **137**, 553–597, <https://doi.org/10.1002/qj.828>.
- Ding, Y. H., C. Li, and Y. Liu, 2004: Overview of the South China Sea monsoon experiment. *Adv. Atmos. Sci.*, **21**, 343–360, <https://doi.org/10.1007/BF02915563>.
- Fang, G., W. D. Fang, Y. Fang, and K. Wang, 1998: A survey of studies on the South China Sea upper ocean circulation. *Acta Oceanogr. Taiwan.*, **37**, 1–16.
- , H. Chen, Z. Wei, Y. Wang, X. Wang, and C. Li, 2006: Trends and interannual variability of the South China Sea surface winds, surface height, and surface temperature in the recent decade. *J. Geophys. Res.*, **111**, C11S16, <https://doi.org/10.1029/2005JC003276>.
- Fang, W., G. Fang, P. Shi, Q. Huang, and Q. Xie, 2002: Seasonal structures of upper layer circulation in the southern South China Sea from in situ observations. *J. Geophys. Res.*, **107**, 3202, <https://doi.org/10.1029/2002JC001343>.
- Farris, A., and M. Wimbush, 1996: Wind-induced Kuroshio intrusion into the South China Sea. *J. Oceanogr.*, **52**, 771–784, <https://doi.org/10.1007/BF02239465>.
- Gan, J., and T. Qu, 2008: Coastal jet separation and associated flow variability in the southwest South China Sea. *Deep-Sea Res. I*, **55**, 1–19, <https://doi.org/10.1016/j.dsr.2007.09.008>.
- He, Y., J. Xie, and S. Cai, 2016: Interannual variability of winter eddy patterns in the eastern South China Sea. *Geophys. Res. Lett.*, **43**, 5185–5193, <https://doi.org/10.1002/2016GL068842>.
- Hsin, Y. C., C. R. Wu, and S. Y. Chao, 2012: An updated examination of the Luzon Strait transport. *J. Geophys. Res.*, **117**, C03022, <https://doi.org/10.1029/2011JC007714>.
- Hu, J., and X. H. Wang, 2016: Progress on upwelling studies in the China seas. *Rev. Geophys.*, **54**, 653–673, <https://doi.org/10.1002/2015RG000505>.
- , H. Kawamura, H. Hong, and Y. Qi, 2000: A review on the currents in the South China Sea: Seasonal circulation, South China Sea warm current and Kuroshio intrusion. *J. Oceanogr.*, **56**, 607–624, <https://doi.org/10.1023/A:101117531252>.
- Hwang, C., and S. A. Chen, 2000: Circulations and eddies over the South China Sea derived from TOPEX/Poseidon altimetry. *J. Geophys. Res.*, **105**, 23 943–23 965, <https://doi.org/10.1029/2000JC900092>.
- Jia, Y., and E. P. Chassignet, 2011: Seasonal variation of eddy shedding from the Kuroshio intrusion in the Luzon Strait. *J. Oceanogr.*, **67**, 601, <https://doi.org/10.1007/s10872-011-0060-1>.
- Kao, H. Y., and J. Y. Yu, 2009: Contrasting eastern-Pacific and central-Pacific types of ENSO. *J. Climate*, **22**, 615–632, <https://doi.org/10.1175/2008JCLI2309.1>.
- Li, L., W. D. Nowlin Jr., and J. L. Su, 1998: Anticyclonic rings from the Kuroshio in the South China Sea. *Deep-Sea Res. I*, **45**, 1469–1482, [https://doi.org/10.1016/S0967-0637\(98\)00026-0](https://doi.org/10.1016/S0967-0637(98)00026-0).
- Liang, W. D., Y. J. Yang, T. Y. Tang, and W. S. Chuang, 2008: Kuroshio in the Luzon Strait. *J. Geophys. Res.*, **113**, C08048, <https://doi.org/10.1029/2007JC004609>.
- Lin, X., C. Dong, D. Chen, Y. Liu, J. Yang, B. Zou, and Y. Guan, 2015: Three-dimensional properties of mesoscale eddies in the South China Sea based on eddy-resolving model output. *Deep-Sea Res. I*, **99**, 46–64, <https://doi.org/10.1016/j.dsr.2015.01.007>.
- Linkin, M. E., and S. Nigam, 2008: The North Pacific Oscillation–west Pacific teleconnection pattern: Mature-phase structure and winter impacts. *J. Climate*, **21**, 1979–1997, <https://doi.org/10.1175/2007JCLI2048.1>.
- Liu, Q., A. Kaneko, and J. L. Su, 2008: Recent progress in studies of the South China Sea circulation. *J. Oceanogr.*, **64**, 753–762, <https://doi.org/10.1007/s10872-008-0063-8>.
- Liu, Y., C. Dong, Y. Guan, D. Chen, J. McWilliams, and F. Nencioli, 2012: Eddy analysis in the subtropical zonal band of the North Pacific Ocean. *Deep-Sea Res. I*, **68**, 54–67, <https://doi.org/10.1016/j.dsr.2012.06.001>.
- Metzger, E. J., 2003: Upper ocean sensitivity to wind forcing in the South China Sea. *J. Oceanogr.*, **59**, 783–798, <https://doi.org/10.1023/B:JOCE.0000009570.41358.c5>.
- , and H. E. Hurlburt, 2001: The nondeterministic nature of Kuroshio penetration and eddy shedding in the South China Sea. *J. Phys. Oceanogr.*, **31**, 1712–1732, [https://doi.org/10.1175/1520-0485\(2001\)031<1712:TNNOKP>2.0.CO;2](https://doi.org/10.1175/1520-0485(2001)031<1712:TNNOKP>2.0.CO;2).
- Nan, F., H. Xue, and F. Yu, 2015: Kuroshio intrusion into the South China Sea: A review. *Prog. Oceanogr.*, **137**, 314–333, <https://doi.org/10.1016/j.pocean.2014.05.012>.
- Nencioli, F., C. Dong, T. Dickey, L. Washburn, and J. C. McWilliams, 2010: A vector geometry–based eddy detection algorithm and its application to a high-resolution numerical model product and high-frequency radar surface velocities in the Southern California Bight. *J. Atmos. Oceanic Technol.*, **27**, 564–579, <https://doi.org/10.1175/2009JTECHO725.1>.
- Nof, D., Y. Jia, E. Chassignet, and A. Bozec, 2011: Fast wind-induced migration of Leddies in the South China Sea. *J. Phys. Oceanogr.*, **41**, 1683–1693, <https://doi.org/10.1175/2011JPO4530.1>.
- Okubo, A., 1970: Horizontal dispersion of floatable particles in the vicinity of velocity singularities such as convergences. *Deep-Sea Res. Oceanogr. Abstr.*, **17**, 445–454, [https://doi.org/10.1016/0011-7471\(70\)90059-8](https://doi.org/10.1016/0011-7471(70)90059-8).
- Pedlosky, J., 1982: *Geophysical Fluid Dynamics*. Springer-Verlag, 626 pp., <https://doi.org/10.1007/978-3-662-25730-2>.
- Pujol, M. I., Y. Faugère, G. Taburet, S. Dupuy, C. Pelloquin, M. Ablain, and N. Picot, 2016: DUACS DT2014: The new multi-mission altimeter data set reprocessed over 20 years. *Ocean Sci.*, **12**, 1067–1090, <https://doi.org/10.5194/os-12-1067-2016>.
- Qu, T., 2000: Upper-layer circulation in the South China Sea. *J. Phys. Oceanogr.*, **30**, 1450–1460, [https://doi.org/10.1175/1520-0485\(2000\)030<1450:ULCITS>2.0.CO;2](https://doi.org/10.1175/1520-0485(2000)030<1450:ULCITS>2.0.CO;2).
- , Y. Y. Kim, M. Yaremchuk, T. Tozuka, A. Ishida, and T. Yamagata, 2004: Can Luzon Strait transport play a role in conveying the impact of ENSO to the South China Sea? *J. Climate*, **17**, 3644–3657, [https://doi.org/10.1175/1520-0442\(2004\)017<3644:CLSTPA>2.0.CO;2](https://doi.org/10.1175/1520-0442(2004)017<3644:CLSTPA>2.0.CO;2).
- , Y. Du, G. Meyers, A. Ishida, and D. Wang, 2005: Connecting the tropical Pacific with Indian Ocean through South China Sea. *Geophys. Res. Lett.*, **32**, L24609, <https://doi.org/10.1029/2005GL024698>.
- , Y. T. Song, and T. Yamagata, 2009: An introduction to the South China Sea throughflow: Its dynamics, variability, and

- application for climate. *Dyn. Atmos. Oceans*, **47**, 3–14, <https://doi.org/10.1016/j.dynatmoce.2008.05.001>.
- Rasmusson, E. M., and T. H. Carpenter, 1982: Variations in tropical sea surface temperature and surface wind fields associated with the Southern Oscillation/El Niño. *Mon. Wea. Rev.*, **110**, 354–384, [https://doi.org/10.1175/1520-0493\(1982\)110<0354:VITSSST>2.0.CO;2](https://doi.org/10.1175/1520-0493(1982)110<0354:VITSSST>2.0.CO;2).
- Rogers, J. C., 1981: Spatial variability of seasonal sea level pressure and 500 mb height anomalies. *Mon. Wea. Rev.*, **109**, 2093–2106, [https://doi.org/10.1175/1520-0493\(1981\)109<2093:SVOSSL>2.0.CO;2](https://doi.org/10.1175/1520-0493(1981)109<2093:SVOSSL>2.0.CO;2).
- Shaw, P. T., S. Y. Chao, and L. L. Fu, 1999: Sea surface height variations in the South China Sea from satellite altimetry. *Oceanol. Acta*, **22**, 1–17, [https://doi.org/10.1016/S0399-1784\(99\)80028-0](https://doi.org/10.1016/S0399-1784(99)80028-0).
- Soong, Y. S., J. H. Hu, C. R. Ho, and P. P. Niiler, 1995: Cold-core eddy detected in South China Sea. *Eos, Trans. Amer. Geophys. Union*, **76**, 345–347, <https://doi.org/10.1029/95EO00209>.
- Sun, Z., Z. Zhang, W. Zhao, and J. Tian, 2016: Interannual modulation of eddy kinetic energy in the northeastern South China Sea as revealed by an eddy-resolving OGCM. *J. Geophys. Res. Oceans*, **121**, 3190–3201, <https://doi.org/10.1002/2015JC011497>.
- Trenberth, K. E., W. G. Large, and J. G. Olson, 1990: The mean annual cycle in global ocean wind stress. *J. Phys. Oceanogr.*, **20**, 1742–1760, [https://doi.org/10.1175/1520-0485\(1990\)020<1742:TMACIG>2.0.CO;2](https://doi.org/10.1175/1520-0485(1990)020<1742:TMACIG>2.0.CO;2).
- Walker, G. T., and E. W. Bliss, 1932: World weather V. *Mem. Roy. Meteor. Soc.*, **4**, 53–84.
- Wang, B., R. Wu, and X. Fu, 2000: Pacific–East Asian teleconnection: How does ENSO affect East Asian climate? *J. Climate*, **13**, 1517–1536, [https://doi.org/10.1175/1520-0442\(2000\)013<1517:PEATHD>2.0.CO;2](https://doi.org/10.1175/1520-0442(2000)013<1517:PEATHD>2.0.CO;2).
- , F. Huang, Z. Wu, J. Yang, X. Fu, and K. Kikuchi, 2009: Multi-scale climate variability of the South China Sea monsoon: A review. *Dyn. Atmos. Oceans*, **47**, 15–37, <https://doi.org/10.1016/j.dynatmoce.2008.09.004>.
- Wang, C., W. Wang, D. Wang, and Q. Wang, 2006: Interannual variability of the South China Sea associated with El Niño. *J. Geophys. Res.*, **111**, C03023, <https://doi.org/10.1029/2005JC003333>.
- Wang, D., H. Xu, J. Lin, and J. Hu, 2008: Anticyclonic eddies in the northeastern South China Sea during winter 2003/2004. *J. Oceanogr.*, **64**, 925–935, <https://doi.org/10.1007/s10872-008-0076-3>.
- , and Coauthors, 2013: Progress of regional oceanography study associated with western boundary current in the South China Sea. *Chin. Sci. Bull.*, **58**, 1205–1215, <https://doi.org/10.1007/s11434-012-5663-4>.
- Wang, G., J. Su, and P. C. Chu, 2003: Mesoscale eddies in the South China Sea observed with altimeter data. *Geophys. Res. Lett.*, **30**, 2121, <https://doi.org/10.1029/2003GL018532>.
- , D. Chen, and J. Su, 2008: Winter eddy genesis in the eastern South China Sea due to orographic wind jets. *J. Phys. Oceanogr.*, **38**, 726–732, <https://doi.org/10.1175/2007JPO3868.1>.
- Wang, L., C. J. Koblinksky, and S. Howden, 2000: Mesoscale variability in the South China Sea from the TOPEX/Poseidon altimetry data. *Deep-Sea Res. I*, **47**, 681–708, [https://doi.org/10.1016/S0967-0637\(99\)00068-0](https://doi.org/10.1016/S0967-0637(99)00068-0).
- Wang, S. Y., M. L'Heureux, and H. H. Chia, 2012: ENSO prediction one year in advance using western North Pacific sea surface temperatures. *Geophys. Res. Lett.*, **39**, L05702, <https://doi.org/10.1029/2012GL050909>.
- Wang, Y., G. Fang, Z. Wei, F. Qiao, and H. Chen, 2006: Interannual variation of the South China Sea circulation and its relation to El Niño, as seen from a variable grid global ocean model. *J. Geophys. Res.*, **111**, C11S14, <https://doi.org/10.1029/2005JC003269>.
- Weiss, J., 1991: The dynamics of enstrophy transfer in two-dimensional hydrodynamics. *Physica D*, **48**, 273–294, [https://doi.org/10.1016/0167-2789\(91\)90088-Q](https://doi.org/10.1016/0167-2789(91)90088-Q).
- Wu, C. R., and Y. C. Hsin, 2012: The forcing mechanism leading to the Kuroshio intrusion into the South China Sea. *J. Geophys. Res.*, **117**, C07015, <https://doi.org/10.1029/2012JC007968>.
- , P. T. Shaw, and S. Y. Chao, 1999: Assimilating altimetric data into a South China Sea model. *J. Geophys. Res.*, **104**, 29 987–30 005, <https://doi.org/10.1029/1999JC900260>.
- Xia, Q., and H. Shen, 2015: Automatic detection of oceanic mesoscale eddies in the South China Sea. *Chin. J. Oceanol. Limnol.*, **33**, 1334–1348, <https://doi.org/10.1007/s00343-015-4354-9>.
- Xiu, P., F. Chai, L. Shi, H. Xue, and Y. Chao, 2010: A census of eddy activities in the South China Sea during 1993–2007. *J. Geophys. Res.*, **115**, C03012, <https://doi.org/10.1029/2009JC005657>.
- Yi, J., Y. Du, Z. He, and C. Zhou, 2014: Enhancing the accuracy of automatic eddy detection and the capability of recognizing the multi-core structures from maps of sea level anomaly. *Ocean Sci.*, **10**, 39–48, <https://doi.org/10.5194/os-10-39-2014>.
- Yu, J. Y., and H. Y. Kao, 2007: Decadal changes of ENSO persistence barrier in SST and ocean heat content indices: 1958–2001. *J. Geophys. Res.*, **112**, D13106, <https://doi.org/10.1029/2006JD007654>.
- , and S. T. Kim, 2011: Relationships between extratropical sea level pressure variations and the central Pacific and eastern Pacific types of ENSO. *J. Climate*, **24**, 708–720, <https://doi.org/10.1175/2010JCLI3688.1>.
- , and —, 2013: Identifying the types of major El Niño events since 1870. *Int. J. Climatol.*, **33**, 2105–2112, <https://doi.org/10.1002/joc.3575>.
- , H. Y. Kao, and T. Lee, 2010: Subtropics-related interannual sea surface temperature variability in the central equatorial Pacific. *J. Climate*, **23**, 2869–2884, <https://doi.org/10.1175/2010JCLI3171.1>.
- , M. M. Lu, and S. T. Kim, 2012: A change in the relationship between tropical central Pacific SST variability and the extratropical atmosphere around 1990. *Environ. Res. Lett.*, **7**, 034025, <https://doi.org/10.1088/1748-9326/7/3/034025>.
- , X. Wang, S. Yang, H. Paek, and M. Chen, 2017: The changing El Niño–Southern Oscillation and associated climate extremes. *Climate Extremes: Patterns and Mechanisms*, *Geophys. Monogr.*, Vol. 226, Amer. Geophys. Union, 1–38, <https://doi.org/10.1002/9781119068020.ch1>.
- Yuan, D., W. Han, and D. Hu, 2006: Surface Kuroshio path in the Luzon Strait area derived from satellite remote sensing data. *J. Geophys. Res.*, **111**, C11007, <https://doi.org/10.1029/2005JC003412>.
- , —, and —, 2007: Anti-cyclonic eddies northwest of Luzon in summer–fall observed by satellite altimeters. *Geophys. Res. Lett.*, **34**, L13610, <https://doi.org/10.1029/2007GL029401>.
- Zhang, H., A. Clement, and P. Di Nezio, 2014: The South Pacific meridional mode: A mechanism for ENSO-like variability. *J. Climate*, **27**, 769–783, <https://doi.org/10.1175/JCLI-D-13-00082.1>.
- Zhang, W., G. A. Vecchi, H. Murakami, G. Villarini, and L. Jia, 2016: The Pacific meridional mode and the occurrence of tropical cyclones in the western North Pacific. *J. Climate*, **29**, 381–398, <https://doi.org/10.1175/JCLI-D-15-0282.1>.
- Zhang, Y., K. R. Sperber, and J. S. Boyle, 1997: Climatology and interannual variation of the East Asian winter monsoon: Results from the 1979–95 NCEP/NCAR reanalysis. *Mon. Wea. Rev.*, **125**, 2605–2619, [https://doi.org/10.1175/1520-0493\(1997\)125<2605:CAIVOT>2.0.CO;2](https://doi.org/10.1175/1520-0493(1997)125<2605:CAIVOT>2.0.CO;2).